Journal of Magnetism and Magnetic Materials 341 (2013) 165–172

Contents lists available at SciVerse ScienceDirect

Journal of Magnetism and Magnetic Materials

journal homepage: www.elsevier.com/locate/jmmm

Annealing induced low coercivity, nanocrystalline Co–Fe–Si thin films exhibiting inverse cosine angular variation

T. Hysen [a,1], Salim Al-Harthi [b], I.A. Al-Omari [b], P. Geetha [a], R. Lisha [a], R.V. Ramanujan [c], D. Sakthikumar [d], M.R. Anantharaman [a,*]

[a] Department of Physics, Cochin University of Science and Technology, Cochin 682022, Kerala, India
[b] Department of Physics, Sultan Qaboos University, PC 123, Muscat, Sultanate of Oman
[c] School of Materials Engineering, Nanyang Technological University, Singapore 639798, Singapore
[d] Graduate School of Interdisciplinary New Science, Toyo University, Kawagoe, Saitama, Japan

ARTICLE INFO

Article history:
Received 27 November 2012
Received in revised form
6 April 2013
Available online 18 April 2013

Keywords:
Magnetic thin film
Kondorsky
Surface morphology
Coercivity
PSD
Surface magnetism

ABSTRACT

Co–Fe–Si based films exhibit high magnetic moments and are highly sought after for applications like soft under layers in perpendicular recording media to magneto-electro-mechanical sensor applications. In this work the effect of annealing on structural, morphological and magnetic properties of Co–Fe–Si thin films was investigated. Compositional analysis using X-ray photoelectron spectroscopy and secondary ion mass spectroscopy revealed a native oxide surface layer consisting of oxides of Co, Fe and Si on the surface. The morphology of the as deposited films shows mound like structures conforming to the Volmer–Weber growth model. Nanocrystallisation of amorphous films upon annealing was observed by glancing angle X-ray diffraction and transmission electron microscopy. The evolution of magnetic properties with annealing is explained using the Herzer model. Vibrating sample magnetometry measurements carried out at various angles from 0° to 90° to the applied magnetic field were employed to study the angular variation of coercivity. The angular variation fits the modified Kondorsky model. Interestingly, the coercivity evolution with annealing deduced from magneto-optical Kerr effect studies indicates a reverse trend compared to magetisation observed in the bulk. This can be attributed to a domain wall pinning at native oxide layer on the surface of thin films. The evolution of surface magnetic properties is correlated with morphology evolution probed using atomic force microscopy. The morphology as well as the presence of the native oxide layer dictates the surface magnetic properties and this is corroborated by the apparent difference in the bulk and surface magnetic properties.

1. Introduction

Soft magnetic thin films are a hot topic of research due to their wide ranging applications in various fields such as magnetic recording, MEMS, sensors, etc., [1–3]. Soft magnetic properties are related to various factors such as alloy composition, nature of magnetic phase, crystal structure, crystal size and annealing conditions. In this context, Co–Fe based materials assume importance, owing to their high saturation magnetization and promising high frequency characteristics. The $Co_{70}Fe_{30}$ composition is thermodynamically stable in the bcc crystal structure [4]. This composition [4] is close to the maximum of spin polarization and possesses the maximum magnetic moment, as shown by the Slater Pauling curve [5]. Combination of these properties makes compositions near to $Co_{70}Fe_{30}$ suitable for various applications such as spin injection systems in spintronic devices [6].

Si can be added to Co–Fe alloys to facilitate amorphisation as well as to tune the magnetic properties. If the material can be tailored in to nanocrystalline thin films then they can be integrated in microelectronic devices. Co–Fe/Co–Fe–Si based metallic glasses are available commercially and these materials can be processed itnto nanocrystalline form by thermal annealing and they possess excellent soft magnetic properties, suitable for applications in transformer cores and magnetic shielding. Amorphous thin films of Fe–Ni/Fe–Ni–B which were subsequently processed into nanocrystalline form by annealing were recently reported [7–13]. However amorphous/nanocrystalline thin films of Co–Fe–Si have not been studied in detail or are seldom reported. Hence a detailed investigation of the nanocrystallization and change of magnetic properties of Co–Fe–Si thin films with thermal annealing was conducted.

Co–Fe thin films are usually prepared on different seed layers to reduce their coercivity. Thomson et al. reported coercivity of 16 Oe for Co–Fe films grown on Au/MgO seed layers [14]. Platt et al. reported coercivity of 12 Oe for Co–Fe films deposited on CoO. They showed that domain walls in the soft films have relatively large mobility in response to changing magnetic fields below the nominal H_c. They also attributed the observed low coercivity values

* Corresponding author. Tel.: +91 4842577404.
E-mail addresses: hysenthomas@gmail.com (T. Hysen), mra@cusat.ac.in (M.R. Anantharaman).
[1] On deputation from Department of Physics, Christian College, Chengannur, Kerala, India.

0304-8853/$ - see front matter © 2013 Elsevier B.V. All rights reserved.
http://dx.doi.org/10.1016/j.jmmm.2013.04.032

to the averaging of the high anisotropy energy [15]. Vopsaroiua et al. reported the dependence of coercivity on grain size for 20 nm Co–Fe thin films prepared by sputtering. They observed a reduction in the coercivity from 120 Oe for samples with a mean grain size larger than 17 nm down to 12 Oe for a sample with a mean grain size of 7.2 nm [16]. Ji reported the growth and physical properties of epitaxial $Co_{70}Fe_{30}$ thin films on Si substrate with a TiN buffer layer. They also reported that the films prepared at 450 °C exhibit a biaxial stress up to 0.52%. The films were reported to have a small in-plane biaxial anisotropy, low coercivity of 23 Oe for film thickness greater than 30 nm [17]. In the above mentioned investigations, the magnetic properties were explained using the Random Anisotopy model (RAM) initially proposed by Alben et al. [18] and modified by Herzer [19]. According to Herzer, excellent soft magnetic properties can be realized, if the size of the individual magnetic domain is reduced to the exchange coupling length (*L*ex). The subsequent exchange coupling results in very low local anisotropies and demagnetization effect. Hence for a large number of exchange coupled nanocrystalline grains, the local anisotropy K_1 is small, resulting in lowering of coercivity. Thus, Co–Fe films can be prepared with very low coercivity by the deposition of an under layer or upper layer of an cobalt ultrathin cobalt oxide. Most of the earlier reports focus on the bulk magnetic property of films, probed using VSM. Hence, detailed investigations, comparing, the surface and bulk magnetic properties of Co–Fe–Si thin films are yet another motivation for this work.

There are several reports on the magnetization reversal mechanism in soft magnetic thin films [6,17]. The Stoner–Wolfarth model based on coherent rotation [20] and the Kondorsky model based on domain wall motion/unpinning [21] are the two important models used for explaining the angular variation of coercivity. Even though one expects structures with sizes below the single domain size to obey the coherent rotation model, size dependent behavior was also observed [22]. In most ferromagnetic materials magnetization reversal is affected by domain nucleation and growth. In the coherent rotation model one assumes that the magnetic vectors rotate collectively with the applied field before reaching saturation. In contrast, the Kondorsky model assumes that magnetization reversal is primarily affected by nucleation and growth of reverse domains or the strong pinning of domains at local defects and inhomogeneities and predicts a $1/\cos\theta$ dependence of coercivity, where θ is the angle between the easy axis and the applied magnetic field. The Herzer model predicts similar coercivity variations for magnetization reversal by coherent rotation and domain wall motion/unpinning models [19].

Even though the Kondorsky model was originally derived for explaining the angular variation of coercivity in hard magnetic materials [21], similar behavior has been observed in many soft magnetic systems [23,24]. Thomson et al. [25] reported that the magetisation reversal of large soft magnetic islands of Co–Pt takes place by nucleation of a 180° reverse domain, followed by the spread of a domain wall throughout the islands. Delalande et al. observed the Kondorsky type angular variation of reduced coercivity in soft magnetic Co–Pt systems with perpendicular anisotropy [26]. Streubel et al. modeled the angular variation of magetisation reversal in Fe–Ni caps by the modified Kondorsky relation [27]. Spiridis et al., based on magnetic studies conducted on Co thin films of various thicknesses, reported that as film thickness decreases, the magetisation reversal mechanism can change from coherent rotation to domain wall movement [28]. Liu et al. reported the Kondorsky type dependence in cobalt thin films [29]. The in plane easy axis coercivity variation with grain size in [15–17] Co–Fe thin films was explained using the Herzer model. However no systematic investigation regarding the easy to hard axis magnetization reversal of Co–Fe-Si thin films has been reported in the literature. Hence investigations on the angular variation of magnetization reversal in Co–Fe–Si thin films assume significance.

We report the deposition of magnetic thin films of Co–Fe–Si on glass and NaCl substrates and the evolution of their magnetic properties with thermal annealing. The films exhibit onset of nanocrystallisation and grain growth with annealing. Further the morphology shows a profound change with annealing which is reflected in change in surface magnetic properties investigated using the magneto-optical Kerr effect (MOKE). The Herzer model is invoked to explain the observed soft magnetic properties of ultra-thin magnetic films. The angular variation of coercivity from in plane to out of plane shows an inverse cosine relationship exhibiting a Kondorsky type variation. The magnetization reversal is primarily governed by the pinning of domains at local defects.

2. Experimental

Thin films were vacuum evaporated using tungsten filaments at a vacuum of 10^{-6} Torr on NaCl and chemically cleaned glass substrates. A composite target with a composition corresponding to $Co_{69}Fe_4Ni_1Mo_2B_{12}Si_{12}$ was used for evaporation. Samples deposited on NaCl were used for TEM analysis. The thicknesses of the deposited films were determined using a Dektac 6M Stylus Profiler. The thin film samples were annealed at 100, 300 and 400 °C for 1 h under a high vacuum of 10^{-6} Torr to avoid possible surface oxidation. GXRD measurements were carried out on the annealed and pristine samples using a Bruker D8 Discover diffractometer with monochromatic Cu Kα X-rays at a grazing incidence angle of 0.5° and wavelength 1.5414 Å. XPS study of the films deposited on float glass substrates was performed with an Omicron Nanotechnology XPS system with monochromatic Al Kα radiation ($h\upsilon = 1486.6$ eV) of source voltage 15 kV and emission current of 20 mA. All scans were carried out at an ultrahigh vacuum of 1.5×10^{-10} Torr. The obtained XPS spectra were deconvoluted and quantified using Casa XPS program (Casa Software Ltd., UK), in which the background was simulated using the Shirley function and the peaks were fitted using a Gaussian Lorentzian function. The spectrum recorded was corrected using the binding energy of adventitious carbon at 284.6 eV and the accuracy of the measured binding energy values is estimated to be ± 0.2 eV. The elemental composition of the sample is extracted from the wide scan, while the individual element peaks were analyzed to obtain the chemical composition. As charging effects are unavoidable in the XPS study of thin films deposited on non-conducting samples, charge compensation was performed by electron gun flooding. The nanoscale imaging was performed using atomic force microscopy (AFM) (Digital Instruments Nanoscope V) in the tapping mode, using ultrahigh resolution cantilevers made of tungsten having radius of less than 1 nm and force constant of 46 N/m. Room temperature magnetization measurements were carried out using VSM (DMS 1660 VSM) with field varying from −10 to +10 kOe. The angular variation of magnetization is recorded by measuring the magnetization with the sample positioned at different angles with respect to the applied field. When the field is along the plane of film the angle is 0° and out of plane the angle is 90°. The surface magnetic properties were probed using a MOKE setup, operated using a red laser with 6328 Å wavelength from a He–Ne laser source. The loops were recorded with a magnetic field applied along the in plane direction.

3. Results

3.1. Composition analysis

The average thickness of the films was found to be 54 nm using the stylus profilometer.

The XPS studies (Fig. 1) conducted on the prepared thin films clearly show the presence of cobalt, iron, oxygen, silicon and boron. Quantification of the spectra of as prepared sample suggested that the surface has a composition of 43.84 wt% Co, 24.50 wt% Fe, 1.36 wt % Si, 3.6 wt% B and 26.70 wt% O. The XPS spectra recorded after further sputtering by Argon ions with energy 3 keV for 30 min (Fig. 1) show a composition of 64.64 wt% Co, 30.60 wt% Fe, 0.34 wt% Si, 0.02 wt% B and 4.40 wt% O. In short the above analysis shows that the pristine film has a native oxide layer of oxides of Co, Fe, and Si and a small percentage of B (slow scan spectra is available as supplementary material).

3.2. Structural analysis

The GXRD pattern of the pristine sample (Fig. 2a) show a broad peak at 44.4° indicating the absence of long range ordering. This is unexpected since $Co_{1-x}Fe_x$ alloy was reported to have good crystalline nature over the entire compositional range. Our result can be explained by assuming that the film is composed of nanocrystalline grains dispersed in an amorphous matrix [7]. It should also be borne in mind that the film contains small amounts of silicon and boron which are the elements typically used in metallic glasses to facilitate the formation of amorphous structure.

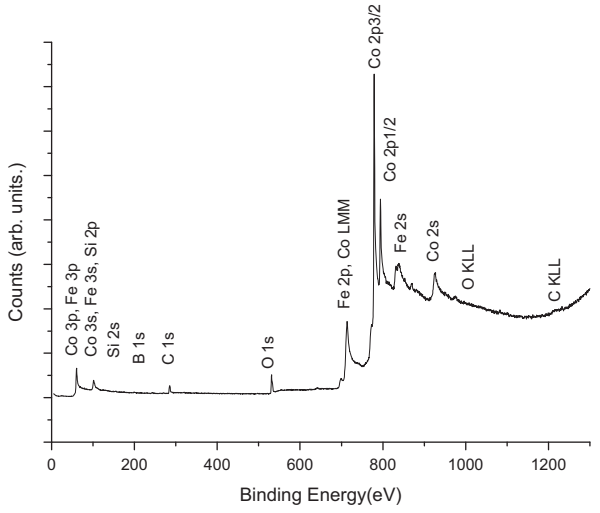

Fig. 1. XPS spectra of Co–Fe–Si film after sputtering with Ar^+ ions for 30 min.

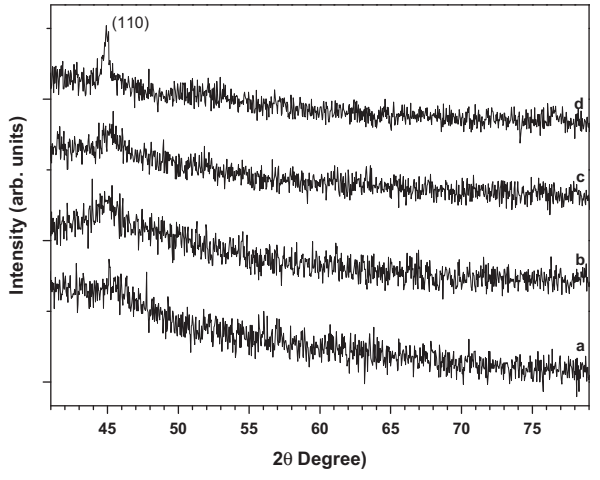

Fig. 2. GXRD pattern of thin film (a) pristine, (b) annealed at 100 °C, (c) 300 °C and (d) 400 °C.

The samples show crystallinity with annealing which is evident from Fig. 2b–d which corresponds to films annealed at temperatures of 100 °C, 300 °C and 400 °C. The peak at 44.4° has a *d* spacing of 2.04 Å. The film annealed at 100 °C, 300 °C and 400 °C shows crystallites with sizes of 5.3 nm, 11 nm and 19.1 nm respectively. The crystallites were found to be made up of Co–Fe by GXRD and TEM measurements and the results were communicated elsewhere.

3.3. Morphology analysis

The magnetic properties of thin films are dependent on the morphology and AFM is a powerful tool for investigating this aspect. The recorded image was subjected to various analyses to obtain information regarding average roughness (R_a), root mean square roughness (R_q), skewness, and power spectral density (PSD). R_a represents the mean value of the surface height with respect to a center plane whereas R_q is the standard deviation of the surface height within the given area [30]. PSD can provide information regarding short and long wavelength ordering in the sample.

The R_a, R_q and *Sku* values derived from the AFM (Figs. 3 and 4) for the substrate and the pristine as well as annealed films are tabulated in Table 1. The substrate has some uneven surface features with an average roughness of 0.94 nm and root mean square roughness of 1.19 nm typical for float glass substrates. The R_a and R_q of Co-Fe-Si thin films gradually reduce upon annealing. This is possible since the films are annealed in high vacuum, the native oxide layer may have smoothened out by diffusion and possibly reduced in thickness due to oxygen depletion. The skewness (*Sku*) value of glass substrate is nearly zero implying uniform distribution of surface features. As deposited film shows a *Sku* value of 0.56 nm suggesting the presence of a wide distribution of small mounds/peaks on the surface. Annealed samples exhibited an increase in *Sku* value whereas the roughness decreases. This suggests the formation of larger flat structures on the film surface which can simultaneously reduce roughness and increase *Sku*. The increase in the *Sku* value with annealing indicates the presence of surface structures, perhaps due to grain coarsening and surface diffusion resulting from annealing. Analysis of XPS spectra of the sample annealed at 300 °C (not included in this manuscript) also showed that the wt% of Co is 40.67, Fe is 39.9, O is 16.91, Si is 2.9 and B is 0.25. Compared to the unsputtered sample the annealed sample has 37% less oxygen and 60% more iron on the surface. The surface also shows more silicon and less boron content. Thus it can be assumed that surface smoothening is driven by the increased presence of silicon and iron on the surface and oxygen depletion resulting from vacuum annealing.

3.4. Bulk magnetic studies using VSM

The magnetic properties of soft magnetic thin films depend on various properties such as morphology, magnetostriction,

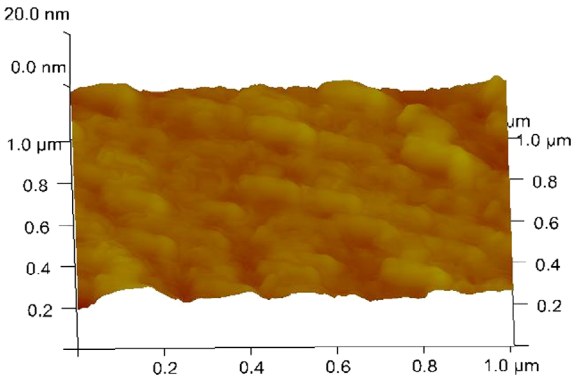

Fig. 3. 3D AFM image of glass substrate.

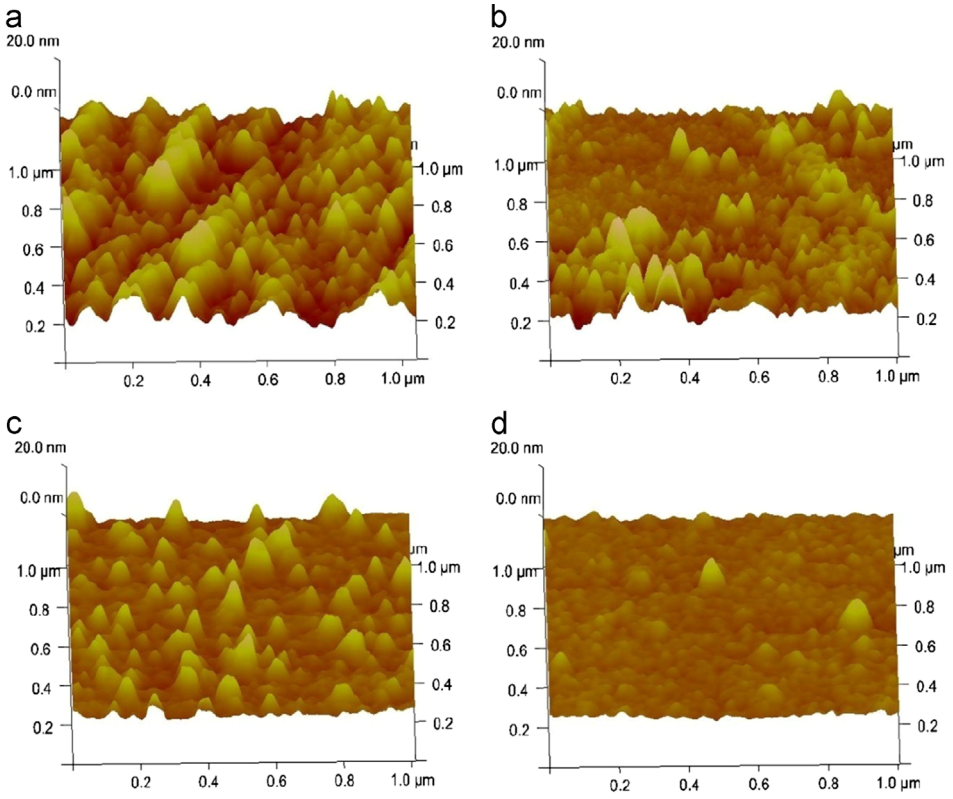

Fig. 4. 3D AFM image Co–Fe–Si films (a) pristine, (b) annealed at 100 °C, (c) annealed at 300 °C and (d) annealed at 400 °C

Table 1
Average roughness (R_a), root mean square roughness (R_q) and Skewness (Sku) values derived from the AFM images for the substrate and the pristine as well as annealed films.

Sample	R_q (nm)	R_a (nm)	Skewness (nm)
Glass substrate	1.19	0.94	0.16
Pristine	3.46	2.76	0.56
Annealed at 100 °C	2.68	1.95	1.29
Annealed at 300 °C	2.21	1.59	1.72
Annealed at 400 °C	1.11	0.748	2.39

magnetic anisotropy, stress, volume fraction of the precipitates and composition.

Fig. 5 shows the variation of coercivity with annealing temperature, measured along the in plane direction. The variation in coercivity can be attributed to the structural as well as morphological changes in the sample with annealing. The coercivity of the pristine film is only 23 Oe. The coercivity shows an initial decrease to 20 Oe at 100 °C annealing due to stress relaxation. As the film is annealed at 300 °C and 400 °C the coercivity shows a gradual increase from 40 to 69 Oe. This can be explained in light of the crystal size increase observed from GXRD.

4. Discussion

4.1. Surface evolution during annealing

The morphology of the as deposited films show mound like structures which suggests the growth mode of films is the Volmer–Weber or island like. It is clear from the 3D AFM that, as the films are annealed from 100 °C to 400 °C the mound like structures progressively decreases, possibly due to surface smoothening resulting from surface diffusion of adatoms.

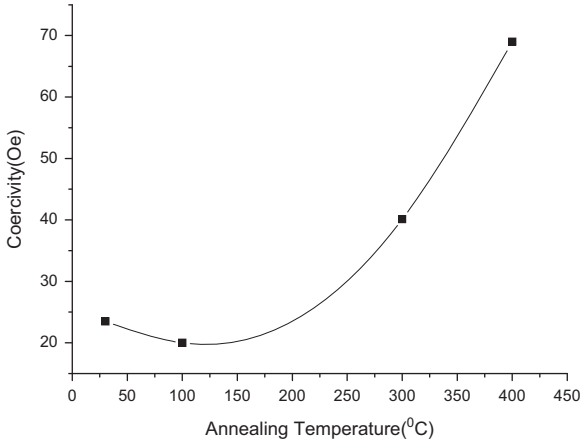

Fig. 5. Variation of coercivity with annealing temperature for Co–Fe–Si films from VSM measurements

The 2D PSD of the bare glass substrates as well as pristine and annealed samples are shown in Fig. 6. The slopes of the PSD spectrum in the high frequency region obeys a power law with slope 4.42, 5.42, 5.38, 5.94, 6.02 for bare glass, pristine film and films annealed from 100 °C, 300 °C to 400 °C, respectively. The negative slope of the high frequency region δ is related to the roughness exponent α by the relation $\alpha = \delta - d/2$, where d is the dimension from which PSD is extracted [31]. In this work $d=2$ which yields α values of 1.21, 1.71, 1.69, 1.97 and 2.01 for bare glass, pristine film and films annealed from 100 °C, 300 °C and 400 °C respectively. The values show a progressive increase except for the pristine film. The R_a and R_q values show a decreasing trend with annealing whereas the roughness exponents show the reverse trend.

The observed α values are quite different from the Kadar Parisi Zhang (KPZ) model which predict a value of α~0.4. [32]. These exponents values can be interpreted using the Wolf–Villian linear

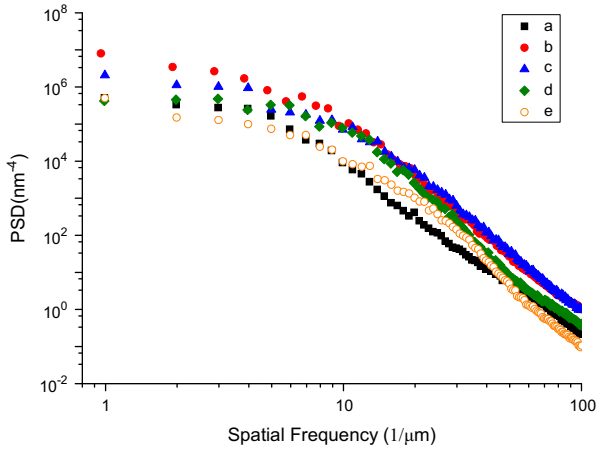

Fig. 6. PSD spectra of (a) bare glass substrate; Co–Fe–Si films (b) pristine, (c) annealed at 100 °C, (d) annealed at 300 °C, and (e) annealed at 400 °C.

diffusion model [33]. According to their model $\partial h/\partial t = R_D - \upsilon\nabla^4 h + \eta$ where the function $h(x,y)$ represents the surface height at points x and y. R_D is the deposition rate which also represents the coalescence/diffusion rate at the surface, υ is a constant and η represents the roughening process with stochastic features. The above equation describes the surface evolution as a competition between kinetic roughening, diffusion driven smoothening and grain coalescence. $\upsilon\nabla^4 h$ represents the surface smoothening by diffusion. This model gives a roughness exponent of $\alpha = 1$. The α values greater than 1 usually indicate the existence of nonlinear effects. Nonlinear diffusion effects can be incorporated into the equation by adding the nonlinear diffusion factor $\lambda\nabla^2(\nabla h^2)$, where λ is a constant related to the growth velocity [34]. This newly inserted nonlinear term takes care of particles that moved to overhangs at the sides of high steps. This new equation predicts roughness exponent values close to 1.5 which is close to the values observed by us in this study. This suggests the possible existence of nonlinear diffusion effects in the system during annealing. This also suggests that the diffusing atoms are preferentially deposited over the valleys, resulting in the film smoothening. As the films are annealed from 100 to 400 °C the roughness exponent increases from 1.69 to 2.71, suggesting the existence of nonlinear surface diffusion effects in the system, leading to surface smoothening. The PSD also shows a small change in slope after q values of 100, which can be ascribed to the fact that the resolution of AFM tip corresponds to a q value of 100 and hence the change in slope after 100 may be due to possible tip artifacts.

4.2. Exchange averaging and 2D-Herzer model for coercivity evolution in film plane

Fig. 5 is similar to the variation reported for the Random Anisotropy model (RAM). The low values of coercivity and anisotropy along the in plane direction suggest exchange averaging. The change in coercivity with crystal size can be modeled by RAM [18,19]. Fenineche reported that Co–Fe alloy films obey RAM [35]. According to RAM, the exchange averaged anisotropy is given by Eq. (2). The parameter A represents the exchange stiffness constant and K_1 the uniaxial anisotropy. The exchange correlation length is given by

$$L_{ex} = \sqrt{\frac{A}{K_1}} \tag{1}$$

$$\langle K\rangle = \frac{K_1^4}{A^3} D^6 \tag{2}$$

implying that the mean anisotropy is proportional to the sixth root of the average crystal size. It follows that for $D < L_{ex}$

$$H_c = \frac{p_c\langle K\rangle}{M_s} = p_c \frac{K_1^4 D^6}{M_s A^3} \tag{3}$$

Also for $D \cong L_{ex}$

$$H_c = \frac{p_c K_1}{M_s} \tag{4}$$

In the above equation p_c acts as a fitting parameter and M_s is the saturation magnetization. These equations are derived assuming a three dimensional material of volume L_{ex}^3. Inserting typical values $K_u \approx 0.27$ kJ/m^3 and $A \approx 9.11 \times 10^{-14}$ J/m^2 for Co–Fe in Eq. (1) gives $L_{ex} \approx 18.4$ nm [16]. Hence in such alloys, if the crystal separation is less than this ≈18.4 nm the anisotropies are averaged out over several crystals and the sample exhibits good soft magnetic properties. However, when one of the dimensions of the material is restricted to values comparable to this typical length scale the system can be approximated as a two dimensional system and the relevant equations are

$$\langle K\rangle = \frac{K_1^2}{A} D^2 \tag{5}$$

$$H_c = \frac{p_c\langle K\rangle}{M_s} = p_c \frac{K_1^2 D^2}{M_s A} \tag{6}$$

All the parameters refer to the same meaning discussed earlier, but they are now the two dimensional counter parts of the corresponding three dimensional values. This equation suggests that for ultra-thin films the D^2 law should be used instead of the D^6 law [36].

The above equation suggests that $\ln(H_c)$ is directly proportional to $\ln(D)$, under the assumption that saturation magnetization is the same for all the samples. The linear plot of $\ln(H_c)$ is directly proportional to $\ln(D)$ (Fig. 7) and confirms that coercivity indeed obeys a D^2 behavior rather than a D^6 behavior. The as prepared samples as well as samples annealed at 100 °C and 300 °C obey the Herzer relation. They have crystal sizes less than the exchange length of 18.4 nm. However the sample annealed at 400 °C has a crystal size greater than the exchange length. This can account for the deviation of the data point for the 400 °C annealed sample from the linear plot of $\ln(H_c)$ versus $\ln(D)$. Vopsaroiua et al. also observed a similar variation in Co–Fe thin films [16].

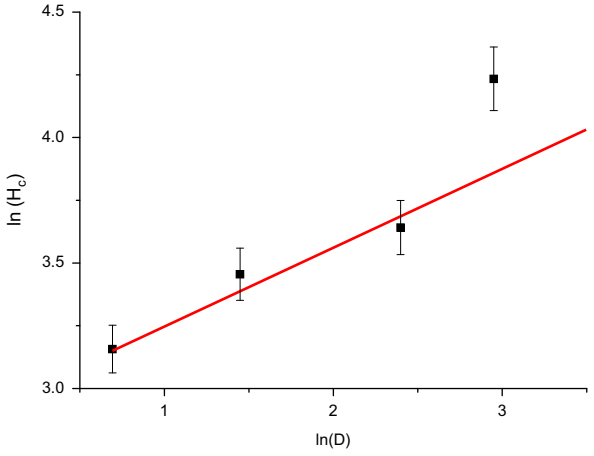

Fig. 7. Plot of $\ln(H_c)$ versus $\ln(D)$

4.3. Angular dependence of coercivity

The angular dependence of coercivity of the as prepared sample is measured by rotating the sample and recording the VSM loops at different angles. By convention it is measured in the angular range of 90°. The in plane hysteresis loop is nearly square, suggesting that coherent rotation of domains or domain wall motion as the dominant mechanism for magnetization reversal. However as the angle changes to 10° and higher values, in addition to domain wall motion a domain rotation process is also operational as seen from the inclination of the magnetization curve before M_s is reached (Fig. 8). At 90° complete saturation cannot be achieved even at the highest fields, suggesting strong uniaxial anisotropy. This supports our use of the two dimensional RAM, which assumes exchange averaging only along the two dimensional surface of the film. It also suggests that magnetization reversal along in plane and out of plane may be due to different mechanisms. It is possible to elucidate the magnetization reversal mechanisms from the angular plot of coercivity.

Generally there are two kinds of magnetization reversal mechanisms (1) coherent rotation, modeled by the Stoner–Wohlfarth (S–W) relation [20] and (2) domain wall motion, modeled by the Kondorsky relation [21]. The angular dependence can also give information about the isolation of crystals since the S–W relation assumes that the crystals are well isolated.

In the case of well isolated crystals, when the field is along the hard axis, the magnetization reversal is dominated by coherent rotation as per the S–W equation.

$$\frac{H_c(\theta)}{H_c(0)} = (\cos^{2/3}\theta + \sin^{2/3}\theta)^{-3/2} \text{ for angles } 0^\circ \le \theta \le 45^\circ$$

$$\frac{H_c(\theta)}{H_c(0)} = \sin(\theta)\cos(\theta) \text{ for angles } 45^\circ \le \theta \le 90^\circ$$

When the magnetization reversal is caused by domain wall motion/reverse domain nucleation, the coercivity follows the Kondorsky model.

$h_c(\theta) = \frac{H_c(\theta)}{H_c(0)} = \sec(\theta)$ for $0^\circ \le \theta \le 90^\circ$ where $H_c(0)$ is the intrinsic coercivity along the easy axis and $h_c(\theta) = \frac{H_c(\theta)}{H_c(0)}$ is the coercivity scaled with the easy axis.

In uniaxial media if the effect of pinning sites has a prominent influence on magnetization reversal, a modified Kondorsky equation [25] can effectively model the reduced coercivity with the angle as $h_c(\theta) = h + \frac{1-h}{\cos(\theta)}$

When the field is applied out of plane, in the as prepared sample, applied magnetic field of 6000 Oe is insufficient to overcome the magnetic anisotropy field. The field reversal is a combination of domain wall motion/unpinning. Along the out of plane direction, the hysteresis loops toward the saturation end is inclined approximately 45° with coercivity of 260 Oe. This may be due to domain pinning effects. The most probable origin of this domain pinning is the presence of a surface oxide layer on top as well as the large surface roughness of the film. The surface oxides can act as pining centers that drag domains from rotating with the applied field. This is manifested as the inclination of the hysteresis curve for the out of plane loops. When the field is applied, the domain wall grows till further alignment along the magnetic field is not possible without domain rotation. According to the Kondorsky theory of domain-wall pinning at a local defect, the coercivity scales as the inverse of the cosine when domain walls grow around a local defect in the process of domain expansion [37].

Fig. 9 shows the variation of scaled coercivity with the angle that the applied field makes with the easy axis. The points suggest a sinusoidal behavior. The red line is the fit of the data points with the modified Kondorsky model. Good fit of the data points indicates that the domain reversal mechanism is primarily Kondorsky type domain wall unpinning from a local defect. As discussed in Section 3.1, the Co–Fe–Si films have a native oxide layer of Co, Fe and Si. The Co and Fe oxides can act as pinning centers for the Co–Fe domains residing underneath. Khan also observed a similar behavior in Cu-capped ultrathin Co films [38].

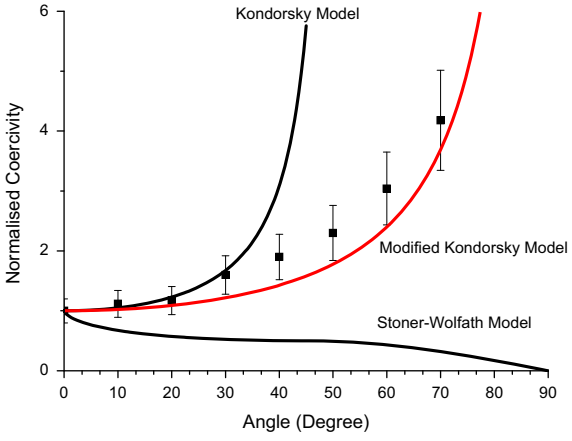

Fig. 9. Plot of the coercivity versus angle for the as prepared film. The thick red line is fit to the data points using the modified Kondorsky model. (For interpretation of the references to color in this figure legend, the reader is referred to the web version of this article.)

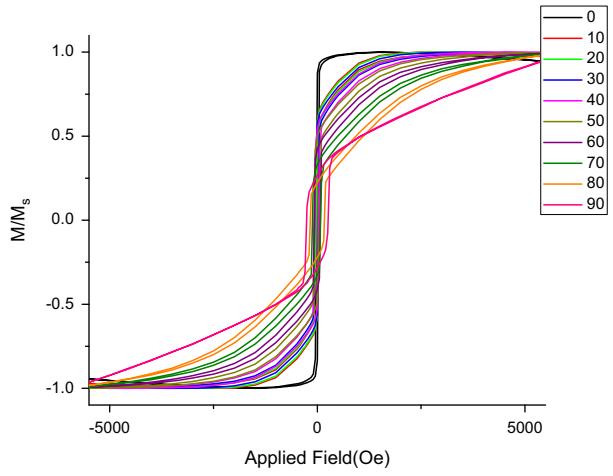

Fig. 8. VSM hysteresis loops of as prepared film for various angles.

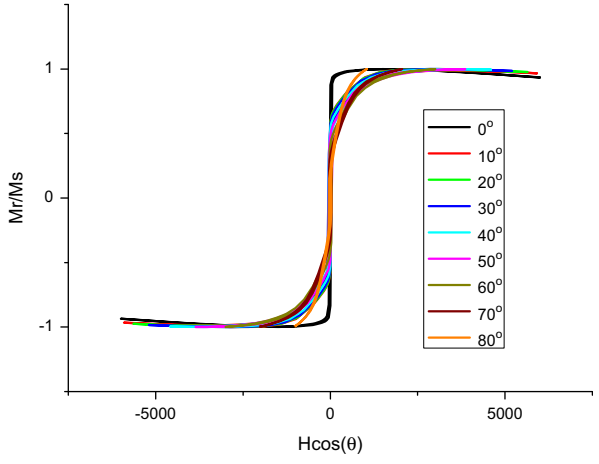

Fig. 10. VSM loops re-plotted by scaling the H values of loops recorded at different angles with $H\cos(\theta)$.

Wei et al. report a mechanism to check the applicability of Kondorsky model [39]. If the hysteresis loops were plotted by scaling the x-axis by $H\cos(\theta)$ for the loops taken at different angles, all the loops should coincide. In our case all loops (Fig. 10), except 0° and 90° coincide with the loop taken at other angles. This provides another proof for the dominance of domain wall motion/unpinning in magnetization reversal. However the in plane loop and out of plane loops do not fit into this category. As the direction of applied field changes from in plane, the magnetization, in addition to the dominant domain wall motion, has to rotate to reach saturation. This is visible by the presence of a small inclination of the loop after remanence. The angular dependence of M–H loops and the reciprocal cosine angle dependence of coercivity clearly show the role of domain wall motion/unpinning in magnetization reversal.

The modified Kondorsky model reproduces the angular dependence of coercivity. However the model is developed on the assumption of a strongly pinned domain before magnetization switching. Rather than pinned domains, incoherent rotation of the domains is a more realistic description of the observed angular dependence. Further the Kondorsky model is generally valid for a continuous film whereas in this work the films, even though continuous, exhibit an island like growth behavior [26]. Uesaka et al. earlier reported that a non-uniform magnetic anisotropy across a particle can produce an asymmetric angular dependence of switching field [40] Spiridis et al. and Kisielewski et al. reported the existence of domain wall motion in magnetization reversal of ultrathin cobalt films [28,41]. Ji also reported the contribution of domain wall motion to magnetization reversal for 10 nm $Co_{70}Fe_{30}$ films along the (100) axis [17]. Chang et al. reported that, Co when exposed to oxygen, can alter its electronic density of states, stress anisotropy and domain wall motion during magnetization reversal [42]. Thus the ultrathin oxide layer serves to pin the magnetic domains of Co–Fe forcing the magnetic reversal mechanism to be domain wall unpinning. This effect is prominent along the out of plane direction.

4.4. Surface magnetic properties

The MOKE hysteresis loops (Fig. 11) show almost square loops with squareness nearly equal to one. However the coercivity evolution (Fig. 12) with annealing temperature from MOKE shows a reverse trend as compared to the bulk VSM loops (Fig. 5). The XPS analysis shows that the films have a thin native oxide layer of iron and cobalt. This oxide layer with a large roughness offers very

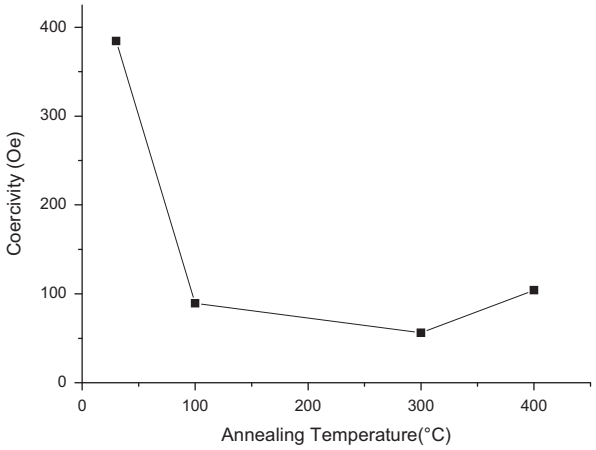

Fig. 12. Variation of surface coercivity with annealing temperature.

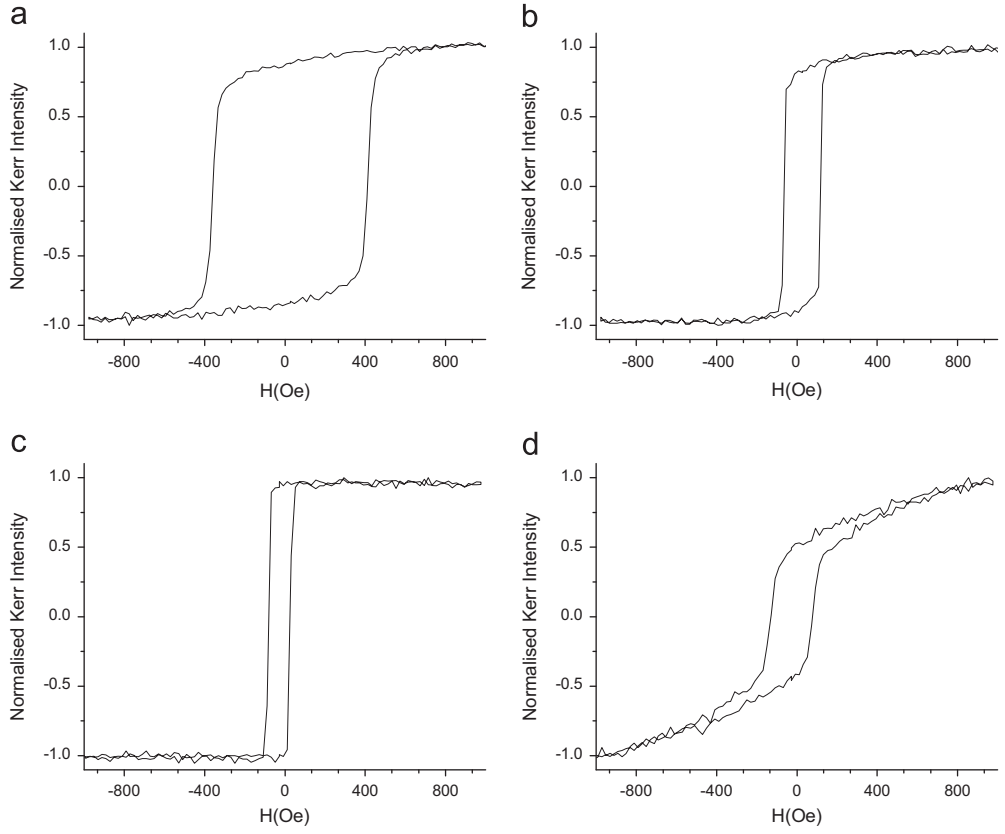

Fig. 11. MOKE loops of films (a) as prepared, (b) annealed 100 °C, (c) annealed 300 °C and (d) annealed 400 °C.

high resistance to domain rotation. The as prepared film has a very high roughness of 3.46 nm. As the film is annealed at 100 °C and 300 °C the roughness values changes from 2.68 nm and 2.21 nm respectively. This suggests possible surface smoothening, annealing out of pinning sites and decrease in thickness of the oxide layer. This can account for the decrease in coercivity.

However, the loop for 400 °C annealed sample is not saturating even at 1000 Oe. Further the shape of the loop suggests that in addition to domain wall motion, domain rotation is also operating. The anisotropy field is also very large. This increased coercivity may be due to the presence of elemental cobalt near the surface. The penetration depth of light is estimated to be <10 nm in metals [43]. Hence it can be expected that the MOKE signals carry magnetic polarization information from the oxide layer as well as the Co–Fe–Si under layer. Since the probing depth of XPS is ~3 nm we can conclude (see supplementary material) that elemental cobalt exists within 3 nm from the surface either as Co or as Co–Fe. Jergel reported such an increase in coercivity for cobalt thin films annealed at 400 °C and explained it by assuming the formation of hcp cobalt crystals [44].

5. Conclusions

Co–Fe–Si thin films prepared by employing thermal evaporation were found to have a native oxide layer on its surface. Annealed thin films were found to behave according to the Herzer model, except for the 400 °C annealed sample. The samples annealed at 400 °C have crystals with a mean size greater than the exchange length, hence possess large coercivity due to the absence of exchange averaging. The angular dependence of coercivity shows that the dominant magnetization reversal mechanism is domain wall unpinning in accordance with the modified Kondorsky model. The bulk and surface magnetic properties were found to be different owing to the presence of a thin oxide layer on the film surface. There is further scope for a detailed investigation comparing the effect of nonmagnetic metallic layers on the surface and bulk magnetic properties of Co–Fe–Si thin films.

Acknowledgments

Fruitful discussions with Dr. Senoy Thomas, Post Doctoral Research Fellow, Cheminitz University, Germany is greatly acknowledged. The authors are thankful to Dr. Sanjay Rai, RRCAT, Indore, for GXRD measurements. HT acknowledges UGC for financial assistance through the FDP Programme. HT acknowledges the financial assistance received from DST FIST to the Department of Physics of his parent institution. GP acknowledges UGC, India, for providing financial assistance in the form of RFSMS Fellowship (No. F4-3/2006(BSR)/8-3/2007(BSR)). LR is thankful to IUAC, New Delhi, for providing financial assistance in the form of UFUP Project. MRA acknowledges financial support through the DST Nano Mission Project. RVR acknowledges the support of NRF CREATE Programme in Nanomaterials for Energy and Water Management and the support of USAOARD office, Tokyo (Programme manager: Dr. K. Caster). IAA acknowledges the Sultan Qaboos University for the support provided in this study under the research Grant no.: IG/SCI/PHYS/12/02

Appendix A. Supplementary materials

Supplementary data associated with this article can be found in the online version at http://dx.doi.org/10.1016/j.jmmm.2013.04.032.

References

[1] S. Ohnuma, H. Fujimori, T. Masumoto, X.Y. Xiong, D.H. Ping, K. Hono, Applied Physics Letters 82 (2003) 946.
[2] Hiroyuki Tagami, Goro Kiyota, IEEE Transactions on Magnetics 41 (2005) 3295.
[3] S.X. Wang, N.X. Sun, M. Yamaguchi, S. Yabukami, Nature 407 (2000) 150.
[4] H. Kikuchi, M. Sato, K. Kobayashi, Journal of Applied Physics 87 (2000) 6055.
[5] R.M. Bozorth, Ferromagnetism, Van Nostrand, New York, 1951.
[6] T. Hindmarch, K. Suszka, M. MacKenzie, J.N. Chapman, M. Henini, D. Taylor, B.J. Hickey, C.H. Marrows, Journal of Applied Physics 105 (2009) 073907.
[7] T. Hysen, S. Deepa, S. Saravanan, R.V. Ramanujan, D.K. Avasthi, P.A. Joy, S.D. Kulkarni, M.R. Anantharaman, Journal of Physics D: Applied Physics 39 (2006) 1993.
[8] S. Thomas, S.H. Al-Harthi, D. Sakthikumar, I.A. Al-Omari, R.V. Ramanujan, Y. Yoshida, M.R. Anantharaman, Journal of Physics D: Applied Physics 41 (2008) 155009.
[9] S. Thomas, S.H. Al-Harthi, R.V. Ramanujan, Zhao Bangchuan, Liu Yan, Wang Lan, M.R. Anantharaman, Applied Physics Letters 94 (2009) 063110.
[10] S. Thomas, S.H. Al-Harthi, I.A. Al-Omari, R.V. Ramanujan, V. Swaminathan, M.R. Anantharaman, Journal of Physics D: Applied Physics 42 (2009) 215005.
[11] S. Thomas, G. Pookat, S.S. Nair, M. Daniel, B. Dymerska, A. Liebig, S.H. Al-Harthi, R.V. Ramanujan, M.R. Anantharaman, Journal of Physics: Condensed Matter 24 (2012) 256004.
[12] T. Hysen, S. Thomas, R.V. Ramanujan, D.K. Avasthi, I.A. Al- Omari, Salim Al-Harthi, M.R. Anantharaman, Nuclear Instruments and Methods in Physics Research B 287 (2012) 85.
[13] S. Thomas, T. Hysen, D.K. Avasthi, A. Tripathi, R.V. Ramanujan, M.R. Anantharaman, Journal of Applied Physics 105 (2009) 033910.
[14] T. Thomson, P.C. Riedi, C.L. Platt, A.E. Berkowitz, IEEE Transactions on Magnetics 34 (1998) 1045.
[15] C.L. Platt, A.E. Berkowitz, D.J. Smith, M.R. McCartney, Journal of Applied Physics 88 (2000) 2058.
[16] M. Vopsaroiua, M. Georgieva, P.J. Grundy, G. Vallejo Fernandez, S. Manzoor, M.J. Thwaites, K. O'Grady, Journal of Applied Physics 97 (2005) 10N303.
[17] C.-X. Ji, Feng Lu, Y. Austin Chang, J. Joshua Yang, M.S. Rzchowski, Applied Physics Letters 92 (2008) 022504.
[18] R. Alben, J.J. Becker, M.C. Chi, Journal of Applied Physics 49 (1978) 1653.
[19] G. Herzer, Physica Scripta 49 (1993) 307;
G. Herzer, IEEE Transactions on Magnetics 26 (1990) 1397.
[20] E.C. Stoner, E.L. Wohlfarth, Philosophical Transactions of the Royal Society of London A 240 (1948) 599.
[21] E. Kondorsky, Journal of Physics Moscow 2 (1940) 161.
[22] Suna Li, Xing Hao, Journal of Applied Physics 104 (2008) 043904.
[23] W.D. Doyle, J.E. Rudisill, S. Shtrikman, Journal of Applied Physics 32 (1961) 1785.
[24] X. Fan, Y.S. Gui, A. Wirthmann, G. Williams, D. Xue, C.M. Hu, Applied Physics Letters 95 (2009) 062511.
[25] T. Thomson, G. Hu, B.D. Terris, Physical Review Letters 96 (2006) 257204.
[26] M. Delalande, J. deVries, L. Abelmann, J.C. Lodder, Journal of Magnetism and Magnetic Materials 324 (2012) 1277.
[27] R. Streubel, D.J. Thurmer, D. Makarov, F. Kronast, T. Kosub, V. Kravchuk, D.D. Sheka, Y. Gaididei, R. Schäfer, O.G. Schmidt, Nano Letters 12 (2012) 3961.
[28] N. Spiridis, T. Slezzak, M. Zajac, J. Korecki, Surface Science 566 (2004) 272.
[29] Z.Y. Liu, S. Adenwalla, IEEE Transactions on Magnetics 39 (2003) 2074.
[30] G. Yildirim, S. Bal, M. Gulen, A. Varilci, E. Budak, M. Akdogan, Crystal Research and Technology 47 (2012) 195.
[31] Junhua Xu, Lihua Yu, Isao Kojima, Journal of Applied Physics 94 (2003) 6827.
[32] M. Kardar, G. Parisi, Y.C. Zhang, Physical Review Letters 56 (1986) 889.
[33] D. Wolf, J. Villian, Europhysics Letters 13 (1990) 389.
[34] D. Aurongzeb, M. Holtz, Menon Latika, Applied Physics Letters 89 (2006) 092501.
[35] N.E. Fenineche, R. Hamzaoui, O. El Kedim, Materials Letters 57 (2003) 4165.
[36] G. Herzer, Materials Science and Engineering: A 133 (1991) 1.
[37] Wei He, Zhan Qing-Feng, Wang De-Yong, Chen Li-Jun, Cheng Zhao-Hua, Chinese Physics B 17 (2008) 1674.
[38] R.A. Khan, A.S. Bhatti, Journal of Magnetism and Magnetic Materials 323 (2011) 340.
[39] Wei He, Zhan Qing-Feng, Wang De-Yong, Chen Li-Jun, Sun Young, Cheng Zhao-Hua, Chinese Physics 16 (2007) 1009.
[40] Y. Uesaka, Y. Nakatani, N. Hayashi, Japanese Journal of Applied Physics 34 (1995) 6056.
[41] M. Kisielewski, Z. Kurant, A. Maziewski, M. Tekielak, N. Spiridis, J. Korecki, Physica Status Solidi A 189 (2002) 929.
[42] H.W. Chang, J.S. Tsay, W.Y. Chang, K.T. Huang, Y.D. Yao, Journal of Magnetism and Magnetic Materials 321 (2009) 2398.
[43] H. Oguchi, A. Zambano, M. Yu, J. Hattrick-Simpers, D. Banerjee, Y. Liu, Z.L. Wang, J.P. Liu, S.E. Lofland, D. Josell, I. Takeuchi, Journal of Applied Physics 105 (2009) 023912.
[44] M. Jergel, I. Cheshko, Y. Halahovets, P. Šiffalovič, I. Mat'ko, R. Senderák, S. Protsenko, E. Majková, Š. Luby, Journal of Physics D: Applied Physics 42 (2009) 135406.